A Mathematical Exploration of the Distance–Redshift Mapping in Cosmology

Jose Parra *

Posted Date: 13 February 2026

doi: 10.20944/preprints202602.1077.v1

Keywords: general relativity; gravitational redshift; relativistic quantum theory; cosmological redshift

 doi:10.20944/preprints202602.1077.v1

Article

A Mathematical Exploration of the Distance–Redshift Mapping in Cosmology

Jose Parra

Florida International University; jlparra@fiu.edu

Abstract

We propose a unified theoretical framework for observed redshift phenomena in astrophysics, in which gravitational and cosmological contributions arise from distinct but coexisting physical mechanisms. In this model, the gravitational field itself carries an effective mass, leading to a nontrivial field–mass structure that naturally identifies halo mass with the gravitational field mass outside baryonic sources. Independently, a cosmological redshift mechanism is derived from a relativistic quantum treatment of coherent photon propagation through an effective medium, resulting in a **nonlinear closed-form energy-loss law** characterized by a single effective parameter with units of Hubble's constant. Through the definition of redshift, these two mechanisms combine multiplicatively, yielding a mathematically consistent total-redshift expression. The framework provides a unified mapping between distance and redshift for both galaxies and quasars without assuming a single dominant redshift cause. The model is constructed from explicit assumptions grounded in relativistic field dynamics and quantum coherence, and its internal consistency is demonstrated through analytic solutions and calibrated examples. Although parameter calibration is used for illustration, it does not constitute empirical validation; the focus is on formal structure, logical coherence, and theoretical plausibility. The proposed framework serves as a basis for future observational tests and theoretical refinement, illustrating how alternative physical interpretations of redshift can be formulated within a consistent relativistic setting.

Keywords: general relativity; gravitational redshift; relativistic quantum theory; cosmological redshift

MSC: 83C05; 83F05; 81Q05

1. Introduction

The increasing precision and observational reach of modern telescopes have produced datasets that expose persistent discrepancies with the predictions of standard cosmological models. These discrepancies, now commonly referred to as *cosmological tensions*, have reached a level of statistical and conceptual significance that motivates consideration of new physical frameworks [1]. One illustrative proposal [2] introduced a novel conceptual approach that, despite criticisms concerning mathematical rigor and structural complexity, achieved sufficient internal coherence to attract serious attention within the astronomical community. Other works [3,4] pursued alternative strategies by formulating scalar potentials within a rigorous mathematical framework, obtaining solutions to the Einstein field equations [5] that exhibit meaningful correspondence with physical observables. Collectively, these results justify the systematic exploration of additional theoretical approaches.

A redshift–distance diagram constructed from galaxy and quasar observations reveals significant deviations from the predictions of the standard ΛCDM cosmological model. The quasar CFHQS J1641+3755 [6], with a measured redshift of $z = 6.047$, is associated with a reported distance modulus of 43.64, corresponding to a comoving distance of approximately 5,346 Mpc. This places the object roughly ~ 5×10^4 Mpc closer than the distance predicted by ΛCDM at the same redshift. Although uncertainties in quasar parameter estimation may contribute to such deviations, analogous

 doi:10.20944/preprints202602.1077.v1

discrepancies are also present in galaxy datasets. For example, the galaxy SDSS-II SN 13151 [7] exhibits a redshift of $z = 0.388$ while being reported at a distance modulus of 48.52, corresponding to approximately 50,583 Mpc—exceeding the ΛCDM prediction by an amount equivalent to a redshift shift of approximately $\Delta z \approx 5.1$. These inconsistencies indicate the presence of either unaccounted systematic effects or fundamental limitations in the current cosmological framework, thereby motivating further theoretical and observational investigation.

A cosmological model [8] motivated by the above-mentioned discrepancies was developed with the objective of minimizing parameter correlations in the description of the observed universe. This simplification was achieved by postulating that the gravitational field possesses an effective mass. As an initial feasibility test, the model adopted a constant-density approximation, constituting a deliberate oversimplification of realistic cosmic matter distributions. In addition, it was incorrectly assumed that the principal model parameters admit no closed-form analytical solutions. The present note corrects this assumption and provides a formal analytical treatment of the model parameters. Furthermore, it introduces a graphical representation designed to facilitate direct comparison between theoretical predictions and observational data.

2. Einstein Field Equations in the Massive-Gravity Cosmological Model

We solve the Einstein field equations subject only to the physical constraints intrinsic to the problem under consideration [9]. Specifically, we impose the following conditions:

1. Spherical symmetry,
2. Static spacetime, and
3. An isotropic perfect fluid with vanishing shear stresses.

Under these assumptions, and adopting the Cartesian signature (+1, +1, +1, -1), the spacetime metric for the squared differential interval ds^2 takes the form:

$$ds^2 = A_{(r)}dr^2 + r^2 d\theta^2 + r^2 \sin^2\theta d\phi^2 - B_{(r)}\left(Cdt\right)^2, \tag{1}$$

here, the function $A_{(r)}$ represents the spatial metric factor, while $B_{(r)}$ denotes the temporal metric factor. The symbol G is the universal gravitational constant, and C denotes the fundamental limiting speed in nature.

No assumptions are introduced beyond those strictly required by the formulation. Empirical evidence supports the existence of a well-defined limiting speed, asymptotically approached by the highest observed velocities, exemplified by the speed of light c. Within this framework, C is treated as a relativistic invariant, while the locally measured value of c is allowed, in principle, to vary with gravitational field strength. This distinction provides a mathematical advantage in the formulation of the model and admits the physical possibility of photon–photon interaction mediated through coherence states of the field.

The explicit field equations for a gravitational configuration with mass density and pressure, derived from general relativity [9] (p. 191) under the assumptions stated above, are given by:

$$-\frac{\hat{\hat{B}}_{(r)}}{2B_{(r)}} + \frac{\hat{B}_{(r)}}{4B_{(r)}}\left(\frac{\hat{A}_{(r)}}{A_{(r)}} + \frac{\hat{B}_{(r)}}{B_{(r)}}\right) + \frac{\hat{A}_{(r)}}{rA_{(r)}} = \frac{4\pi G}{C^4}\left(\rho_{(r)}C^2 - P_{(r)}\right)A_{(r)}, \tag{2}$$

$$1 - \frac{1}{A_{(r)}} + \frac{r}{2A_{(r)}}\left(\frac{\hat{A}_{(r)}}{A_{(r)}} - \frac{\hat{B}_{(r)}}{B_{(r)}}\right) = \frac{4\pi G}{C^4}\left(\rho_{(r)}C^2 - P_{(r)}\right)r^2, \tag{3}$$

$$\frac{\hat{\hat{B}}_{(r)}}{2A_{(r)}} - \frac{\hat{B}_{(r)}}{4A_{(r)}}\left(\frac{\hat{A}_{(r)}}{A_{(r)}} + \frac{\hat{B}_{(r)}}{B_{(r)}}\right) + \frac{\hat{B}_{(r)}}{rA_{(r)}} = \frac{4\pi G}{C^4}\left(\rho_{(r)}C^2 + 3P_{(r)}\right)B_{(r)}, \tag{4}$$

 doi:10.20944/preprints202602.1077.v1

$$\left[1-\frac{1}{A_{(r)}}+\frac{r}{2A_{(r)}}\left(\frac{\hat{A}_{(r)}}{A_{(r)}}-\frac{\hat{B}_{(r)}}{B_{(r)}}\right)\right]\sin^2\theta=\frac{4\pi G}{C^4}\left(\rho_{(r)}C^2-P_{(r)}\right)r^2\sin^2\theta\,, \tag{5}$$

where single and double hats denote first- and second-order derivatives with respect to the radial coordinate, respectively. The function $\rho(r)$denotes the volumetric energy density of the gravitational field, and $P(r)$represents the corresponding isotropic pressure distribution.

By multiplying Equation (2) by [2 $A_{(r)}$]$^{-1}$, Equation (4) by [2 $B_{(r)}$]$^{-1}$, and Equation (3) by r^{-2}, and subsequently summing the resulting expressions, one obtains—after straightforward algebraic manipulation—

$$\frac{d}{dr}\left[\frac{r}{A_{(r)}}\right]=1-\frac{8\pi G}{C^4}\rho_{(r)}C^2r^2\,. \tag{6}$$

Combining Equation (6) with the mass identity

$$m_{(r)}\equiv m_R+\int_R^r 4\pi r^2\rho_{(r)}dr\,, \tag{7}$$

where m_R denotes a gravitational seed of radius R (not necessarily baryonic), biases the spatial factor such that

$$A_{(r)}=\frac{1}{1-\dfrac{2Gm_{(r)}}{C^2r}}\,. \tag{8}$$

The function $B_{(r)}$ must satisfy the constraint arising from the combination of Equation (1) minus Equation (2) times $A_{(r)}$ r^{-2}. Explicitly, it is

$$-\frac{\hat{\hat{B}}_{(r)}}{2B_r}+\left(\frac{1}{2}\frac{\hat{B}_{(r)}}{B_r}\right)^2+\left(\frac{1}{2}\frac{\hat{B}_{(r)}}{B_r}+\frac{1}{r}\right)\frac{\hat{A}_{(r)}}{2A_r}+\frac{\hat{B}_{(r)}}{2rB_r}-\frac{A_r}{r^2}+\frac{1}{r^2}=0\,. \tag{9}$$

The temporal function satisfying Equation (9) is expected to incorporate Schwarzschild's solution for intermediate gravitational intensities, as this solution reduces to Newton's law in the weak-field limit. Substituting Equation (8) and its first derivative into Equation (9) yields the solution

$$B_{(r)}=1-\frac{2Gm_{(r)}}{C^2r}\,, \tag{10}$$

only if the equation

$$r^2\hat{\hat{\rho}}_{(r)}+4r\hat{\rho}_{(r)}-\rho_{(r)}=0 \tag{11}$$

is satisfied. The result exhibits that the Schwarzschild metric emerges as the trivial solution of Equation (11) in the limit $\rho_{(r)}\to 0$, even near $r\to R$. Equation (11) admits two roots: one diverges with increasing radius and is therefore disregarded, while the other

$$\rho_{(r)}=\rho_R\left(\frac{r}{R}\right)^{-\frac{1}{2}\left(\sqrt{13}+3\right)} \tag{12}$$

will be used.

Substituting Equation (12) into Equation (7) imposes the following condition on the mass of the gravitational field:

 doi:10.20944/preprints202602.1077.v1

$$m_{(r)} = m_R \left\{ 1 + \frac{6}{\sqrt{13}-3} \left[1 - \left(\frac{r}{R} \right)^{-\frac{1}{2}\left(\sqrt{13}-3\right)} \right] \right\}. \tag{13}$$

Applying the Lagrange equations to the metric of the model yields three principal results: the orbital circular velocity at the source, the gravitational redshift of photons observed at infinity, and the escape velocity of a particle to the same endpoint. The corresponding expressions are

$$\beta_{orb} = \sqrt{\frac{r\hat{B}_{(r)}}{2B_{(r)}}} = \sqrt{\frac{\frac{Gm_R}{C^2 r}\left\{ 1 + \frac{3}{\sqrt{13}-3} \left[2 - \left(\sqrt{13}-1\right) \left(\frac{r}{R} \right)^{-\frac{1}{2}\left(\sqrt{13}-3\right)} \right] \right\}}{1 - \frac{2Gm_R}{C^2 r} \left\{ 1 + \frac{6}{\sqrt{13}-3} \left[1 - \left(\frac{r}{R} \right)^{-\frac{1}{2}\left(\sqrt{13}-3\right)} \right] \right\}}}, \tag{14}$$

$$z = \sqrt{\frac{1}{B_{(r)}}} - 1 = \frac{1}{\sqrt{1 - \frac{2Gm_R}{C^2 r} \left\{ 1 + \frac{6}{\sqrt{13}-3} \left[1 - \left(\frac{r}{R} \right)^{-\frac{1}{2}\left(\sqrt{13}-3\right)} \right] \right\}}} - 1, \text{ and} \tag{15}$$

$$\beta_{esc} = \sqrt{1 - B_{(r)}} = \sqrt{\frac{2Gm_R}{C^2 r} \left\{ 1 + \frac{6}{\sqrt{13}-3} \left[1 - \left(\frac{r}{R} \right)^{-\frac{1}{2}\left(\sqrt{13}-3\right)} \right] \right\}}. \tag{16}$$

3. Results

3.1. Gravitational Redshift

We now consider the characterization of a super-quasar exhibiting a large redshift despite its proximity. The quasar CFHQS J1641+3755 [6] has a spectroscopic redshift of z = 6.047. Some of its calculated physical parameters [10–12] include a central black hole of mass 2.4 x 10^8 $M_\odot$, a stellar and gas mass of 10^{11} $M_\odot$, and the so-called M_{200c}, defined as the mass enclosed within the radius R_{200c} = 2 x 10^{21} m, where the mean density equals 200 times the critical density at that redshift, yielding 2.4 x 10^{12} $M_\odot$.

According to general relativity, stable circular orbits around a black hole cease to exist interior to the innermost stable circular orbit (ISCO). For a non-spinning (Schwarzschild) black hole, the ISCO radius $6\ G\ M\ C^{-2}$ is approximately equal to 2.1 x 10^{12} m, corresponding to an orbital velocity near 0.41 C at the inner edge of the accretion disk. Further out, in the radiatively efficient portion of the disk (e.g., at R ~ 100 r_g), the Keplerian velocity decreases to approximately 0.1 C. These scalings follow directly from relativistic orbital dynamics [13,14].

We test the model by comparing its predicted values with those expected from well-established theories. Perfect agreement is not required, as the values originate from different frameworks; however, a relative correlation is necessary to support the validity of the new approach.

Assume a central gravitational mass of 2.04 x 10^7 $M_\odot$ enclosed within a radius R = 2.6 x 10^6 m, corresponding to a density of 5.5 x 10^{17} kg m^{-3}. According to Equation (13), at a radius R_{isco} = 4.987 x 10^{12} m, the field mass should be 2.2 x 10^8 $M_\odot$, yielding a total mass of 2.4 x 10^8 $M_\odot$. Furthermore, at radius r, Equations (14–16) predict an orbital velocity of 0.273 C and an escape velocity of 0.362 C.

 doi:10.20944/preprints202602.1077.v1

Any radiation emitted from the R_{ISCO} experiences an energy decrement due to the gravitational pull of the mass enclosed within the R_{ISCO}, as well as additional reductions resulting from the stellar, dust, gas, and gravitational contributions encountered along its path away from the quasar. The modeling of this total mass is constructed to approach the previously defined M_{200c} asymptotically. The following equation formalizes this behavior:

$$m_{(r)} = \left\{ m_{risco} + m_{200c} \left[1 - e^{-(r - r_{isco})\mathbb{R}^{-1}} \right] \right\} M_{\odot} . \tag{17}$$

A total of one million steps were performed to compute the fraction of energy remaining at a final radius of 2.024 x 10^{17} m, assuming an initial energy of 100%. At each step, the mass was calculated using Equation (17) according to

$$m_{(r)} = \left\{ m_{risco} + m_{200c} \left[1 - e^{-(n-1)\mathbb{R}^{-1} dr} \right] \right\} M_{\odot} , \tag{18}$$

here, the constant $\mathbb{R}$ = 2.000 x 10^{16} m, the counter n runs from 1 to 10^6, and the step size is dr = 4.987 x 10^{12} m. The remaining energy fraction at each step is then computed as

$$E_n = E_{n-1} \sqrt{\left\{ 1 - \frac{2Gm_{(r)}}{C^2 \left[r_{isco} + (n-1)dr \right]} \right\} \left[1 - \frac{2Gm_{(r)}}{C^2 \left(r_{isco} + ndr \right)} \right]^{-1}} . \tag{19}$$

As mentioned previously, E_0 = 100%. The resulting gravitational redshift at the final radius is then z = 5.809 according to

$$z_{grav} = \frac{E_0}{E_{10^6} \sqrt{1 - \frac{2Gm_{\left(r_{isco} + 10^6 dr \right)}}{C^2 \left(r_{isco} + 10^6 dr \right)}}} - 1 . \tag{20}$$

3.2. Cosmological Redshift

Cosmological data from galaxies exhibiting small redshifts, even at large distances, can help constrain the modeling of the cosmological redshift. For example, consider the galaxy SDSS-II SN 13151 [7], introduced in the ***Introduction***. Although this problem has been addressed in detail previously [15], we provide here a streamlined derivation and clarify the adaptation of the main parameters to the formalism used in the present work.

Under the following assumptions:

1. The coherence of the light state depends on the interaction of each photon with surrounding photons in all directions.
2. A universal speed limit C exists. According to special relativity, the speed of light c corresponds to this limit; however, in general, c need not coincide exactly with C, but under the conditions, $c < C$ and may be considered a local variable.
3. The Dirac's equation [16], been relativistic invariant, could be extended to a general expression. Its formalism could be applied to any potential. These potentials could be electrically acting on charges e or could be gravitationally acting on rest masses m.

From assumption 3:

$$i\hbar \frac{\partial \psi}{\partial t} = \left[C\vec{\alpha} \cdot \left(\vec{p} - m\vec{A} \right) - m\phi + \beta mC^2 \right] \psi , \tag{21}$$

here, $i^2 = -1$, $\hbar$ is the reduced Planck constant ($h/2\pi$), ψ is the state function, and t denotes time. The vector $\boldsymbol{\alpha}$ is a 4 x 4 matrix containing the Pauli matrices, $\boldsymbol{p}$ is the four-momentum vector, ϕ and $\boldsymbol{A}$ are

 doi:10.20944/preprints202602.1077.v1

the gravitational scalar and vector potentials, respectively (with $\boldsymbol{A} = 0$ for photons due to their spin-1 nature), and β is another 4 x 4 matrix populated with positive and negative ones and zeros.

Applying cylindrical coordinates to Equation (21) yields four coupled equations, whose solutions indicate that a beam of photons propagating in a coherent state must lose energy. The corresponding effect, expressed as a redshift in the notation adopted throughout this paper, is

$$z_{\text{cosm}} = \sqrt{1 + \frac{mC^2}{\hbar c} d} - 1, \tag{22}$$

here, d denotes the distance traveled by the photon beam. Equation (22) exhibits several notable conditions that, in principle, support the validity of its derivation. First, Planck's constant $\hbar$ cannot be zero; otherwise, any photon would lose all its energy immediately upon interaction with another photon. This is consistent with the quantum condition that photons cannot exist in the limit $\hbar \to 0$. Second, if $c = C$, implying that the photon mass is zero, photons would retain their energy regardless of travel distance, as it is assumed now.

It is intriguing to note that $m\, C^2\, \hbar^{-1}$ approximates $2\, H_0$ when Equation (22) is expanded for small distances d, consistent with Hubble's law. This equivalence would hold if all galactic and quasar redshifts were purely cosmological; however, such a scenario is not assumed in the present analysis.

It is convenient to combine the three constants in Equation (22) into a single effective constant, as shown below,

$$z_{\text{cosm}} = \sqrt{1 + \frac{2\text{X}}{c} d} - 1, \tag{23}$$

here, $X \equiv \text{m C}^2\, \hbar^{-1}$ represents the photon energy leakage rate and has the same units as Hubble's constant.

3.3. Total Redshift

The redshift is defined as the fractional difference between the emitted energy and the detected energy, minus one. Performing the algebra and neglecting other physical effects, such as the Doppler effect, yields the following relationship:

$$z_{tot} = \left(z_{grav} + 1\right)\left(z_{\text{cosm}} + 1\right) - 1. \tag{24}$$

The value of X was determined by adjusting the model to ensure that all quasar and galaxy redshifts shown in Figure 1 were reproduced by Equation (24). The figure reveals a semi-symmetric distribution of quasars and galaxies, including objects with relatively low redshifts that follow a similar semi-linear trend as those with higher redshifts.

The two independent parameters in Equation (24), X and the maximum gravitational redshift, are defined by the extrema of the quasar and galaxy distribution. Specifically, $X = 2$ km s^{-1} Mpc^{-1}, and the maximum gravitational redshift is $z_{grav\_max} = 5.8$. The lower bound is anchored by the galaxy SDSS-II SN 13151, while the upper bound is determined by the quasars CFHQS J1641+3755, ULAS J1120+0641, J1342+0928, and the galaxy GRB 090429B, as illustrated in Figure (1).

For the quasar CFHQS J1641+3755, Equation (23) predicts a cosmological redshift of $z_{cosm} = 0.035$. Combined with a gravitational redshift of $z_{grav} = 5.809$, the total redshift according to Equation (24) is $z_{tot} = 6.047$, in agreement with the observed value [6].

It should be emphasized that this agreement does not constitute a validation of the model. The coincidence of model and observed redshifts was obtained by manually adjusting the parameter $\mathbb{R}$ in Equation (18), demonstrating that the model can, in principle, account for the observed redshift.

 doi:10.20944/preprints202602.1077.v1

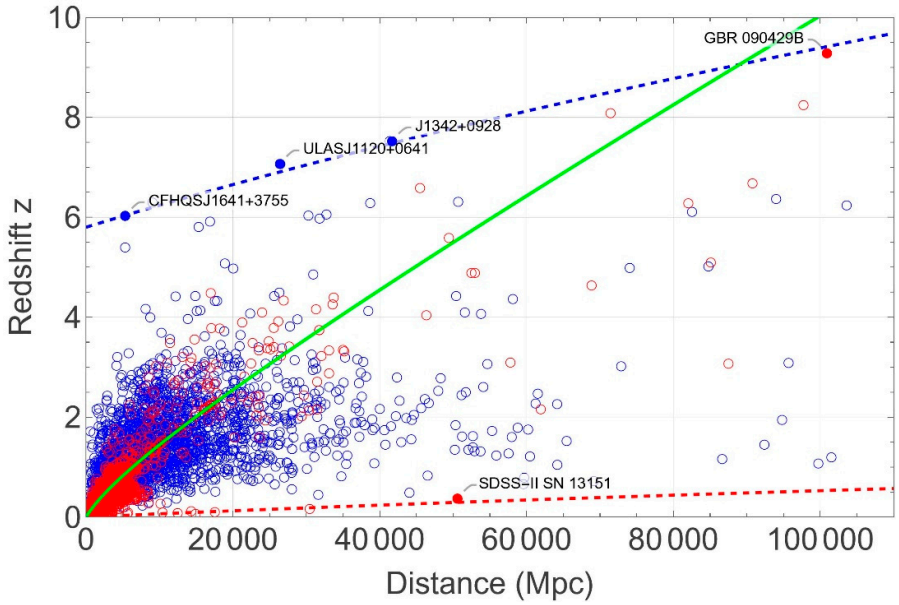

Figure 1. Redshift–distance relation for 2,417 quasars [6,17–19] (blue circles) and 6,880 galaxies [7] (red circles), together with two models. The green curve was generated with the assistance of OpenAI's ChatGPT-13, calibrated to the ΛCDM model with parameters H_0 = 73 Km s^{-1} Mpc^{-1}, Ω_m = 0.3, and Ω_Λ = 0.7. The dashed red and blue curves correspond to Equation (24) with a gravitational redshift of 0 and 5.8, respectively. The model reproduces all displayed points when X = 2 Km s^{-1} Mpc^{-1}.

4. Discussion

The number of galaxies and quasars in the universe, the range of their distances from the observer, and the spread of redshift detected in their emitted radiation are sufficiently large that the underlying explanation must be as simple as possible. Nevertheless, it is unsurprising that a single cause may not account for all observed phenomena. A natural next step is to consider a combination of two causes; however, this approach introduces the challenge of determining whether their contributions are additive, multiplicative, or otherwise coupled. Alternatively, one may posit a single physical mechanism that manifests differently across distinct locations or times—for instance, one effect could be local, while the other is non-local.

In the present work, our central hypothesis is that any field possesses mass. According to the principles of relativity, this implies that any speed associated with such fields must be, at least microscopically, less than the universal speed limit. The consequences of this assumption vary according to the dynamics of each field, as detailed below.

Locally, if the gravitational field possesses mass, its density and pressure will be dominated by the baryonic matter in solid or liquid form, as recently discussed [4]. In this paper, a new solution to the general relativity equations outside a baryonic source was introduced. Specifically, it was found that the function describing the gravitational field at different locations allows the identification of the so-called dark matter mass with the gravitational field mass.

It is assumed that the properties of the gravitational field density are not overridden by the baryonic dust and gas within it, but rather coexist under a ratio of approximately ten, consistent with the baryon fraction suppression relative to the cosmic mean [20]. It should be noted that the gravitational field is expected to follow the superposition principle; therefore, the gravitational field mass associated with all local sources, such as stars, can be added linearly.

To illustrate the significance of this halo mass, we consider a quasar example. The calculation shows that, in the absence of halo mass, radiation emitted from the quasar's disk would emerge with a redshift of only 0.066. Observations [10–12], however, indicate a redshift of 5.809, which will be further modified by the coherence state of the light beam during propagation to the detector.

 doi:10.20944/preprints202602.1077.v1

The energetic state of a coherent light beam can be described by solving the relativistic quantum equation for a cylindrical ensemble of energetically coupled particles. Nevertheless, gravitational and cosmological redshifts are physically independent phenomena; their contributions cannot be added linearly due to the standard definition of redshift. Instead, the definition inherently combines these effects multiplicatively, as is typical for correlated processes.

This multiplicative relationship simplifies the modeling, as the astronomical data in Figure (1) exhibits a similar distribution of points at both low and high redshifts. This pattern is consistent with the independent nature of the two mechanisms: although Figure (1) may suggest that the gravitational redshift simply adds to the cosmological redshift, but the energy of the beam is, in fact, first influenced by the local gravitational field of the source and subsequently modified by the coherence state of the beam during propagation.

The static model of the universe presented here is mathematically self-consistent, does not contradict any currently known physical laws, and appears robust with respect to variations in its parameters. To illustrate this assertion, one may consider, for example, the mass of the photon. Equation (25) by expressing this relationship:

$$m = \frac{2X\hbar}{C^2}, \tag{25}$$

implies that the photon mass is constant. Using the constraint that the universal speed limit C exceeds but is extremely close to the speed of light c, yields a photon mass of approximately around 2 $x10^{-70}$ kg. This value is smaller than the currently established upper limit for the photon mass (PMUL = 3 $x10^{-63}$ kg) [21].

Beyond this, the model may primarily serve as a convenient numerical tool for astronomers, rather than providing direct predictive power. This is plausible due to the additive nature of the two contributing factors discussed here. Specifically, if the redshift is dominated by the ΛCDM description, then the gravitational and cosmological contributions considered in the present work—both positive—cannot reduce the ΛCDM values. Consequently, this model is structurally incapable of accounting for the region below the green curve in Figure (1).

If this work proves of interest to readers, it may inspire further investigation of three questions that remain unresolved due to limitations of time and resources:

1. Verifying whether the gravitational solution presented in our model satisfies other general relativity constraints, such as the conservation of energy.
2. Examining whether data from modern telescopes remain consistent with the red and blue dashed curves in Figure (1).
3. Investigating why most galaxies and quasars exhibit a higher concentration near the green curve representing the ΛCDM model in Figure (1).

5. Conclusions

This work presents a theoretical framework in which gravitational, cosmological, and coherence-based mechanisms contribute jointly to observed redshift phenomena. The model is constructed from a small set of physical assumptions: the existence of mass associated with physical fields, relativistic constraints on universal speed limits, and the applicability of relativistic quantum formalisms to coherent photon propagation. These assumptions lead to modified gravitational field dynamics, a nontrivial field-mass structure, and the emergence of multiple redshift channels.

A new solution to the Einstein field equations outside baryonic sources was introduced, allowing the identification of gravitational field mass with effective halo mass. Independently, a cosmological redshift mechanism was derived from a relativistic quantum treatment of coherent photon beams, yielding a nonlinear energy-loss formulation characterized by a single effective parameter. Through the definition of redshift, these mechanisms combine multiplicatively, producing a total redshift expression that is structurally consistent and mathematically well-defined.

 doi:10.20944/preprints202602.1077.v1

The agreement between the model and selected observational data is achieved through parameter calibration and therefore does not constitute empirical validation. The present results should be interpreted as proof of theoretical consistency and internal coherence rather than as observational confirmation. No claim is made that the framework supersedes the ΛCDM model, which remains the standard cosmological description.

The primary contribution of this work lies in establishing a unified formal structure in which multiple redshift mechanisms can coexist without internal contradiction, and in demonstrating that such a structure can be constructed within relativistic and quantum-consistent principles. Future work must focus on observational discrimination, independent parameter determination, consistency with general relativistic conservation laws, and predictive testing against high-precision cosmological datasets to assess the physical viability of the model.

References

1. Valentino, E. et al. The CosmoVerse White Paper: Addressing observational tensions in cosmology with systematics and fundamental physics, Physics of the Dark Universe 2025, 49, 1-263, *DOI: 10.1016/j.dark.2025.101965*.
2. Jusufi, K.; Singleton, D. Regular black holes with gravitational self-energy as dark matter, *ArXiv* **2025**, https://arxiv.org/pdf/2509.13335.
3. Cembranos, J.A.R.; Luis Díaz-Giménez L. Hydrodynamical Misner–Sharp Formulation for Gravitational Collapse in Scalar–Tensor Theories *ArXiv* **2025**, https://arxiv.org/pdf/2512.17526.
4. Das, S.; Radinschi, I.; Chattopadhyay, S. Modified Gravity Description of Neutron Star in the *f*(*R*) Framework. *Axioms* **2023**, *12*, 234. https://doi.org/10.3390/axioms12030234.
5. Einstein, A. The field equations of gravitation, 1er ed., Publisher: *Princeton University Press*, Einstein.papers.press.princeton.edu (Prusian Academy of Science 1914-1917), USA, https://einsteinpapers.press.princeton.edu/vol6-trans/129
6. Ochsenbein, F. The VizieR database of astronomical catalogues, *Publisher Centre de Donnees astronomique de Strasbourg* (CDS) **2020**, https://doi.org/10.26093/cds/vizier.
7. NASA/IPAC Extragalactic Database. 2020. NED30.5.1-D-17.1.2-20200415 V2. *NASA*. https://ned.ipac.caltech.edu/Archive/Distances/ (Accessed on May 22, 2025).
8. Parra, J. L. Quasars as strong standard candle candidates, *International Journal of Modern Physics A* **2025**, 40, 1-8, https://doi.org/10.1142.
9. Walecka, J.D. Introduction to General Relativity, 1st ed., *World Scientific Publishing Co. Pte. Ltd*. **2007**, pp. 190-191.
10. Willott, C.J. *et al*. EDDINGTON-LIMITED ACCRETION ANDTHEBLACKHOLEMASSFUNCTIONATREDSHIFT6. The Astronomical Journal **2010**, 140, pp. 546-560. https://iopscience.iop.org/article/10.1088/0004-6256/140/2/546/pdf
11. Fan, X. *et al*. A SURVEY OF z > 5.8 QUASARS IN THE SLOAN DIGITAL SKY SURVEY. I. DISCOVERY OF THREE NEW QUASARS AND THE SPATIAL DENSITY OF LUMINOUS QUASARS AT z ~ 6. The Astronomical Journal **2001**, 122, pp. 2833-2849. https://iopscience.iop.org/article/10.1086/324111/pdf
12. Venemans, B.P. *et al*. DISCOVERY OF THREE z > 6.5 QUASARSI NTHE VISTA KILO-DEGREE INFRARED GALAXY (VIKING) SURVEY. The Astronomical Journal **2013**, 779, pp. 24-37. http://dx.doi.org/10.1088/0004-637X/779/1/24
13. Shakura, N.I., Sunyaev, R.A. Black Holes in Binary Systems: Observational Appearances. Published online by Cambridge University Press **1973**, pp. 155-164. https://doi.org/10.1017/S007418090010035X
14. Abramowicz, M.A., Fragile, P.C. Foundations of Black Hole Accretion Disk Theory. Living Rev. Relativity **2013**, 16, pp. 1-88, http://www.livingreviews.org/lrr-2013-1
15. Parra, J.L. Photonic Gravitational Interactions from a Quantum Point of View. Optics and Photonics Journal **2021**, 11, pp. 12-21, https://www.scirp.org/pdf/opj_2021012814341831.pdf
16. Dirac, P. The Quantum Theory of the Electron. Proceedings of the Royal Society A. Proc. R. Soc. Lond. **1928**. A 117, 610-624. Doi: 10.1908/rspa. 1928.0023.

 doi:10.20944/preprints202602.1077.v1

17. Lusso, E. Tension with the flat λCDM model from a high-redshift Hubble diagram of supernovae, quasars, and gamma-ray bursts, Astronomy & Astrophysics **2019**, 4 pp. 1-5, https://flore.unifi.it/handle/2158/1173376.
18. E. Lusso, E. Quasars as standard candles III. Validation of a new sample for cosmological studies, *Astron. & Astrop.* **2020**, 642, pp. 1-24, https://www.aanda.org/articles/aa/abs/2020.
19. Risality, G. Cosmological constraints from the Hubble diagram of quasars at high redshifts, *Nature Astronomy* **2019**, 3, pp. 272-277, https://www.nature.com/articles/s41550-018-0657-z.
20. . Aghanim, N., Akrami, Y., Ashdown, M., Aumont, J., Baccigalupi, C., … et al. Planck 2018 results. VI. Cosmological parameters, *Astronomy & Astrophysics*, **2020** ,641, A6. https://doi.org/10.1051/0004-6361/201833910
21. Chibisov, G.V. Astrophysical Upper Limits on the Photon Rest Mass. Soviet Physics Uspekhi **1976**, 19, 624-626. https://doi.org/10.1070/PU1976v019n07ABEH005277